



Title	Comparison of imaging modalities for the accurate delineation of arteriovenous malformation, with reference to stereotactic radiosurgery
Author(s)	Aoyama, Hidefumi; Katoh, Norio; Kudo, Kohsuke et al.
Citation	International Journal of Radiation Oncology Biology Physics, 62(4), 1232-1238 https://doi.org/10.1016/j.ijrobp.2005.03.039
Issue Date	2005-07-15
Doc URL	https://hdl.handle.net/2115/8494
Type	journal article
File Information	J Radiat Oncol Biol Phys 62 pp1232-1238.pdf



Comparison of imaging modalities for the accurate delineation of arteriovenous malformation, with reference to stereotactic radiosurgery

Hidefumi Aoyama, M.D., Ph.D.¹, Hiroki Shirato, M.D., Ph.D.¹, Norio Katoh, M.D.¹, Kohsuke Kudo, M.D., Ph.D.¹, Takeshi Asano, M.D., Ph.D.¹, Satoshi Kuroda, M.D., Ph.D.², Tatsuya Ishikawa, M.D., Ph.D.², and Kazuo Miyasaka, M.D., Ph.D.¹

1. Department of Radiology, Hokkaido University Graduate School of Medicine, Sapporo, Japan
2. Department of Neurosurgery, Hokkaido University Graduate School of Medicine, Sapporo, Japan

Address for correspondence:

Hidefumi Aoyama, M.D., Ph.D.

Department of Radiology, Hokkaido University Graduate School of Medicine, North-15 West-7, Sapporo, Japan, 060-8638

Tel: 81-11-716-1161; Fax: 81-11-706-7876;

hao@radi.med.hokudai.ac.jp

Presented in part at the American Society for Therapeutic Radiology and Oncology (ASTRO) Annual Meeting, Oct 18-23, 2003, Salt Lake City, UT, USA

Page 19, Table 2, Figure 4

Running title: MRA for radiosurgery of AVM

ABSTRACT

Purpose: To investigate the discrepancy between the arteriovenous malformations (AVMs) seen on magnetic resonance angiography (MRA), and seen on stereotactic digital subtracted angiography (DSA).

Materials and Methods: The target volume on stereotactic DSA (V_{DSA}) and the target volume on MRA (V_{MRA}) were separately delineated in 28 intracranial AVMs. The coordinates of the center and the outer edges of V_{DSA} and V_{MRA} were calculated and used for the analyses.

Results: The standard deviations (mean value) of the displacement of centers of V_{MRA} from V_{DSA} were 2.67 mm (-1.82 mm) in the left-right direction, 3.23 mm (-0.08 mm) in the anterior-posterior direction, and 2.16 mm (0.91 mm) in the cranio-caudal direction. V_{MRA} covered less than 80% of V_{DSA} in any dimensions in 9 cases (32%), although no significant difference was seen in the target volume between each method with a mean value of 11.9 cc for V_{DSA} and 12.3 cc for V_{MRA} ($p=0.948$).

Conclusion: The shift of centers between each modality is not negligible. Considering no significant difference between V_{DSA} and V_{MRA} , but inadequate coverage of the V_{DSA} by V_{MRA} , it is reasonable to consider that the target on MRA might include the feeding artery and draining vein, and possibly miss a portion of the nidus.

Key words: Radiosurgery, AVM, MRA, CTA, Angiography, IGRT

INTRODUCTION

Stereotactic radiosurgery of brain lesions requires precise information on the target coordinates and morphology for single or fractionated high-dose application. For treatment planning of intracranial arteriovenous malformations (AVMs), stereotactic angiography has been the basic source of three-dimensional (3D) information of target volume ¹⁻⁵. However, stereotactic angiography with the conventional biplanar technique is limited in its depiction of the 3D anatomy of AVMs ¹. Recent improvements in conformal radiation techniques, such as 3D conformal radiation therapy and intensity modulation radiation therapy, have made it possible to confine the high-dose radiation region to the 3D shape of the target. Because of this, a more precise 3D target shape is now required for radiosurgical planning. Gadolinium-enhanced 3D time-of-flight magnetic resonance angiography (MRA) and computed tomographic angiography (CTA) are the imaging modalities which can provide detailed 3D information on the AVM shape ³⁻¹². However, discrepancies are frequently experienced between the target created on an MRA or CTA, and the target on stereotactic angiography ⁵. The authors of previous publications have attributed the cause of this discrepancy to the poor depiction of AVM on biplanar stereotactic angiography ^{1,3-11}; however, none of these publications compared the targets created only on an MRA with those created only on a stereotactic

angiography. In this study, therefore, we compared the target created on an MRA with the target created on a stereotactic angiography, in order to investigate the possible cause of the discrepancy between these two modalities. The feasibility of the use of CTA with a rapid injection contrast medium from the artery was also evaluated.

MATERIALS AND METHODS

The patients in this study consisted of 26 consecutive patients with intracranial pial AVMs treated between April 2002 and August 2003. One patient who had 3 pial AVMs was included, and thus 28 AVMs were used for evaluation. The median age of the patients was 51 years, and ranged from 13 to 69. There were 16 male and 10 female patients. The twenty-eight AVMs included 5 infratentorial lesions, with the rest being located at the cerebrum. Conventional stereotactic biplanar digital subtracted angiography (DSA) (Advantx LCN, GE, Milwaukee, WI) was conducted on all patients by immobilizing them using a stereotactic frame with fiducial markers attached at the front, back, and sides of the frame. The targets were delineated by a neuroradiologist. The co-ordinates of the center of the nidus and the maximum diameter were calculated using software based on the calculation method proposed by Shidon et al ¹³. The MRA was obtained on a 1.5-Tesla MR scanner with a standard head coil (Magnetom Symphony, Siemens, Erlangen, Germany) on all patients 3-5 days prior to treatment

planning. Three-dimensional time-of-flight MRA was performed after the injection of 0.2 mL of gadodiamide per kilogram of body weight. The imaging parameters were as follows: TR=37 msec, TE=7.15 msec, flip angle=25° , band width=100 Hz per pixel, section thickness=0.5 mm, field of view=150 x 200 mm, matrix=230 x 512, partitions=60, 3 slabs, acquisition time=9 minutes 39 seconds. The total number of sections was 138. The resultant voxel dimensions were 0.9 x 0.4 x 0.5 mm. Magnetization transfer was used. The acquisition volume was placed in an oblique axial direction so that the volume included the whole of the AVM. Computed tomography (CT) for radiation treatment planning (plan-CT) was performed on all patients, with the patient immobilized by the same stereotactic frame by the CT machine (Sfida, SCT-7000TX/TH; Shimazu, Kyoto), with a slice thickness of 3 or 5 mm and a matrix size of 256 x 256 with an FOV of 280 mm. The source data of the MRA was three-dimensionally co-registered to the plan-CT based on 6 to 10 anatomical landmarks on a commercially available registration machine, which has been described elsewhere ¹⁴. The nidus of the AVM was delineated on the MRA co-registered with the plan-CT (**Figure 1**) by radiation oncologists first. Neuroradiologists and neurosurgeons modified the target if necessary. The center and maximum diameter of the nidus were used for this analysis.

In 15 of the 28 AVMs, CTA was performed immediately after stereotactic DSA. A scanner capable of spiral data acquisition with an injection of contrast medium was used (GE IVR Angio CT System, Advantx ACT (Advantx LCN, HiSpeed LX/I), GE, Milwaukee, WI). The contrast medium was given via an intravascular catheter placed in the proximal arteries of the AVMs. The CTA protocol consisted of conventional unenhanced scanning with 5 to 10 mm slice thickness, followed by helical scanning during rapid injection of contrast medium, and finally by conventional delayed postcontrast scanning with 5 to 10 mm slice thickness. Helical scanning was performed using 3-times-diluted contrast medium at a rate of 2.5 ml/s with a prescan delay time determined by the information from the stereotactic DSA. The CTA data was transferred as MRA to plan-CT. The delineation made by the MRA was modified using the CTA data in these 15 patients. The role of the additional information of CTA to MRA was evaluated.

The discrepancy between the target on conventional stereotactic DSA (V_{DSA}) and that on the MRA (V_{MRA}) in the coordinates of the center of the nidus, the maximum diameter, and the volume of the nidus assuming an ellipsoidal shape were measured. The coordinates of the outer edge of the nidus were also measured. If V_{MRA} alone is used to determine the target volume, it may not cover V_{DSA} . This issue was addressed in each dimension by calculating the ratio of the maximum length of the intersection of the V_{MRA}

with the V_{DSA} to the maximum length of the V_{DSA} in that dimension. This calculation was repeated in all three orthogonal dimensions.

RESULTS

Displacement of the centers of targets between V_{DSA} and V_{MRA}

The standard deviation (mean value) of the displacement of the center of V_{MRA} to the center of V_{DSA} was 2.67 mm (-1.82 mm) in the left-right (LR) direction, 3.23 mm (-0.08 mm) in the anterior-posterior (AP) direction, and 2.16 mm (0.91 mm) in the cranio-caudal (CC) direction (**Figures 2a, 2b, 2c**). The root-mean-square displacement, an estimation of 3D distance, was 4.7 +/- 2.9 mm. There were 2 AVMs (7%), of which the 3D displacement was 1cm or more, 6 AVMs (21 %) with the distance ranging from 5 mm to 1cm, 12 AVMs (43%) from 2 mm to 5 mm, and 8 AVMs (29 %) of 2mm or less. No correlation between the size of the nidus and degree of displacement was found (**Figure 3**). Retrospective analysis suggested that the displacement of centers over 1 cm was attributed to the low quality of conventional stereotactic DSA due to the overlapping of major vessels in one case (AVM-12), and to the poor depiction of the MRA in one case (AVM-23).

Size and volume assessment

The mean maximum diameter of V_{DSA} in the LR, AP, and CC directions was 2.206 cm, 2.369 cm, and 2.106 cm, respectively. These values of V_{MRA} were 2.287 cm, 2.632 cm, and

2.138 cm, respectively. The difference was not statistically significant in all directions with P-values of 0.797 for LR, 0.502 for AP, and 0.928 for the CC directions, respectively. The average nidus volume of V_{DSA} was 11.9 cc (range: 0.1-118.1 cc), and that was 12.3 cc (range: 0.20-97.2 cc) in V_{MRA} . The difference was not statistically significant by the analysis of the student t-test ($p=0.948$).

The coverage of V_{DSA} by V_{MRA}

The mean percent coverage of V_{DSA} by V_{MRA} was 88.9% (range: 33-100%) in the LR direction, 90.9% (range: 61.0-100%) in the AP direction, and 91.0% (range: 64-100%) in the CC direction. There were 9 AVMs for which the coverage ratio was less than 80% in any direction (**Table 1**). The low coverage of these 9 AVMs was considered to be attributed to the underestimation by V_{MRA} in 8 AVMs, and the over-estimation on angiography in one patient in the retrospective assessment.

The impact of the use of CTA in addition to MRA

The clarity of visualization of the AVMs was rated for the CTA and MRA separately by a single investigator (H.A). These images were rated “clear” if abnormal vascular structures were easily identified and “unclear” if the abnormal vascular structure was vague and difficult to identify. AVM on CTA was rated “clear” in 13 cases (87%), whereas that on MRA was rated “clear” in 10 cases (67%)(χ -square, $p=0.38$). In cases in which the

visualization of AVM on the MRA was “unclear”, the targets were delineated based on the information provided by either the CTA or plan-CT as a platform of dose calculation. Statistically significant improvement was not observed with regards to the displacement of centers between the V_{MRA} delineated on MRA alone and that did on CTA in addition to MRA (**Table 2**). However, the CTA gave us useful, flow-dynamics-related information in a case of a relatively large AVM (AVM-22), and we omitted the portion of the draining vein from the target (**Figure 4**).

DISCUSSION

In the radiosurgical treatment planning of intracranial AVM, the importance of the integration of 3D-image information on stereotactic angiography has been widely recognized since the 1990's. MRA and CTA have both been investigated for this purpose. Bednarz et al. combined contrast-enhanced time-of-flight MRA and stereotactic angiography in the treatment planning of 22 AVMs ³. They found that the treatment plans were modified in 12 patients (55 %) after inclusion of the MRA data. Kondziolka et al. used MRA for radiosurgical treatment, and found that the MRA provided additional critical information on the shape of the AVM in 16 of 28 (57 %) patients ⁴. They suggested the possibility of doing treatment planning with MRA without conventional angiography. In our study, we discovered that the displacement of centers between V_{MRA} and V_{DSA} was

greater than 5 mm in one-third of the cases, regardless of the size of the AVMs, a fact which has not been well documented in previous publications. In addition, no significant difference was seen between the measurements of V_{MRA} and V_{DSA} . However, the MRA-based target did not adequately cover the angiography-based target in one-third of the cases. Although it is difficult to judge which is more accurate since pathological confirmation of the real shape of the AVM is impractical, the results of this study suggest that the use of MRA alone for the target delineation might lead to missing of some of the target volumes and could result in compromised treatment outcome.

Tanaka et al. evaluated the conspicuity of the nidus by MRA and CTA ¹². They found that MRA failed to discriminate 21 (68 %) of 31 draining veins which were detected by angiography, and that CTA failed to discriminate 12 (50%) of 24 feeding arteries. On the other hand, MRA successfully discriminated 19 (79%) of 26 feeding arteries, and the CTA depicted 18 (78%) of 23 draining veins, but it was not certain whether MRA and CTA could work complementarily to detect the accurate shape of nidus. We addressed this concern by comparing target delineated on MRA alone and one did on CTA in addition to MRA in regard to the discrepancy of centers; however, the results did not suggest that the complementary use of CTA and MRA could reduce the discrepancy of the center coordinates from an angiography-based center. Blatt et al. investigated the issue of the

shift of the nidus center and difference in diameter between the nidus seen on conventional stereotactic angiography, and CT with intra-arterial contrast infusion in 81 AVMs ⁵. In 44 cases (54%), the isocenters differed by an average of 3.6 mm. Fourteen nidi were larger on CT (average, 2.6 mm), and 30 were smaller on CT (average, 4.0 mm). They concluded that those discrepancies could be attributed to error in the angiographic nidus determination, including overlapping vessels, bony structures, fine filamentous arterioles, and an irregular shape. The distortion of DSA could be a possible source of error as well ^{15, 16,17}. Factors that influence the distortions are the curvature of the I/I screen (“pin-cushion distortion”), the earth’s magnetic field (“S distortion”) and other external or internal magnetic fields. Pincushion distortion can be mathematically reduced, but S distortion cannot be eliminated ¹⁵. The distortion can be up to 4 mm at the edge of image without distortion correction, although it is usually 1mm or less for the diameter of 16 – 23 cm from the center of image, therefore the contribution of the distortion correction could be minimal ^{16,17}.

We agree that biplanar stereotactic angiography has some limitations in the depiction of nidus, as Blatt et al. ⁵ and other authors have pointed out ^{1,3,4}. However, we should be aware of limitation of MRA and CTA as well. One of the major drawbacks of these modalities is the limited ability of temporal resolution ^{18,19}. Distortion of images and

some other artifacts inherent to MRA could be the result of other possible source of error as well ^{3,4,5,14,20}. The distortion of MRI happens by system-related and object-related causes and it can be as large as 4-5 mm at the edge of the magnetic field ^{14,20}. System-related distortion can be reduced by the modification of k-space data; however, its contribution is small as far as brain lesions are concerned because the distortion is usually sub-millimeter around the center of magnetic field without distortion-correction ¹⁴.

The results of the present study suggest that the target on MRA or CTA might have included an unnecessary area of the AVM (the feeding artery or draining vein), but missed an important portion (the nidus), probably because of the poor temporal resolution of MRA.

Therefore, our supposition is that DSA still remains the basic source for 3D information to delineate the nidus and to discriminate the feeding arteries and draining veins from the nidus. Two groups have recently reported the advanced use of DSA for targeting purposes. Colombo et al. developed a novel system of integrating non-stereotactic 3D rotational angiography with stereotactic CT scanning ¹⁸. They used their system in 20 patients, and the result was compared to that obtained by conventional biplanar stereotactic angiography. For each patient, the number of

isocenters and the dimension of the selected collimators were the same, based on the information supplied by both methods. Target coordinates were modified in 5 cases by a very limited amount (mean 0.7 mm, range 0.3-1.0 mm). Zhang et al. reconstructed a biplanar stereotactic DSA to a three-dimensional fashion (segmented DSA), and then complementarily used 3-D information in the targeting process ¹⁹. The shift of center between the targets determined on the segmented DSA plus the enhanced CT and classic stereotactic DSA was 0.1-0.2 mm in any direction. Because the shift of centers when the MRA or CTA was used was 2 - 4 mm in our series and in one by Blatt et al. ⁵, using advanced 3D angiography as shown by Colombo et al. Zhang et al. is recommended to improve the accuracy of target delineation.

In conclusion, the use of MRA or CTA provided important 3D information for target determination, but the shift of center between MRA and stereotactic DSA, and inadequate coverage of angiography-based target by MRA-base target were not negligible. Therefore, DSA should be the basic source for 3D information to delineate the nidus. If the target is delineated using an MRA, it is important to understand the limitations of the MRA, in order to ensure delineation of the nidus, and to exclude unnecessary structures in the target volume.

REFERENCES

1. Spiegelmann R, Friedman WA, Bova FJ. Limitations of angiographic target localization in planning radiosurgical treatment. *Neurosurg* 1992; 30: 619-623.
2. Aoyama H, Shirato H, Nishioka T, et al. Treatment Outcome of Single or Hypofractionated Single-isocentric Stereotactic Irradiation (STI) using a Linear Accelerator for Intracranial Arteriovenous Malformation. *Radiother Oncol* 2001; 59: 323-328.
3. Bednarz G, Downes B, Werner-Wasik W, et al. Combining stereotactic angiography and 3D time-of-flight magnetic resonance angiography in treatment planning for arteriovenous malformation radiosurgery. *Int J Radiat Oncol Biol Phys* 2000; 46: 1149-1154.
4. Kondziolka D, Lunsford LD, Kanal E, et al. Stereotactic magnetic resonance angiography for targeting in arteriovenous malformation radiosurgery. *Neurosurg* 1994; 35: 585-591.
5. Blatt DR, Friedman WA, Bova FJ. Modifications based on computed tomographic imaging in planning the radiosurgical treatment of arteriovenous malformation. *Neurosurgery* 1993; 33: 588-596.
6. Schad LR. Improving target volume characterization in stereotactic treatment

planning of brain lesions by using high-resolution BOLD MR-venography. *NMR Biomed* 2001, 41, 478-483.

7. Farb RI, McGregor C, Kim JK, et al. Intracranial arteriovenous malformations: Real-time auto-triggered elliptic centric-ordered 3D gadolinium-enhanced MR angiography - initial assessment. *Radiology* 2001; 220: 244-251.

8. Essig M, Engenhardt R, Knopp MV, et al. Cerebral arteriovenous malformations: improved nidus demarcation by means of dynamic tagging MR-angiography. *Magn Reson Imaging* 1996; 14: 227-33.

9. Morikawa M, Numaguchi Y, Rigamonti D, et al. Radiosurgery for cerebral arteriovenous malformations: assessment of early phase magnetic resonance imaging and significance of gadolinium-DTPA enhancement. *Int J Radiat Oncol Biol Phys* 1996; 34, 663-675.

10. Guo WY, Nordell B, Karlsson B, et al. Target delineation in radiosurgery for cerebral arteriovenous malformations. Assessment of the value of stereotaxic MR imaging and MR angiography. *Acta Radiologica* 1993; 34: 457-463.

11. George EJS, Butler P, Plowman PN. Can magnetic resonance imaging alone accurately define the arteriovenous nidus for gamma knife radiosurgery? *J Neurosurg* 2002; 97 (suppl. 5) 464-470.

12. Tanaka H, Numaguchi Y, Konno S, et al. Initial experience with helical CT and 3D reconstruction in therapeutic planning of cerebral AVMs: Comparison with 3D time-of-flight MRA and digital subtraction angiography. *J Comput Assist Tomogr* 1997; 21, 811-817.
13. Shidon RL, Barth NH. Stereotactic localization of intracranial targets. *Int J Radiat Oncol Biol Phys* 1987;13: 1241-1246.
14. Aoyama H, Shirato H, Nishioka T, et al. Magnetic resonance imaging system for three-dimensional conformal radiotherapy and its impact on gross tumor volume delineation of central nervous system tumors. *Int J Radiat Oncol Biol Phys* 2001; 50: 821-827.
15. Soderman M, Picard C, Ericson K. An algorithm for correction of distortion in stereotaxic digital subtraction angiography. *Neuroradiology*. 1998 May; 40: 277-82.
16. Wu TH, Lee JS, Wu HM, et al. Evaluating geometric accuracy of multi-platform stereotactic neuroimaging in radiosurgery. *Stereotact Funct Neurosurg*. 2002; 78: 39-48.
17. Perks J, St George EJ, Doughty D, et al. Is distortion correction necessary for digital subtraction angiography in the Gamma Knife treatment of intra-cranial arteriovenous malformation? . *Stereotact Funct Neurosurg*. 2001; 76: 94-105.
18. Colombo F, Cavedon C, Francescon P, et al. Three-dimensional angiography for

radiosurgical treatment planning for arteriovenous malformations. *J Neurosurg* 2003; 98: 536-543.

19. Zhang XQ, Shirato H, Aoyama H, et al. Clinical significance of 3D reconstruction of arteriovenous malformation using digital subtraction angiography and its modification with CT information in stereotactic radiosurgery. *Int J Radiat Oncol Biol Phys* 2003; 57: 1392-1399.

20. Khoo VS, Dearnaley DP, Finnigan DJ, et al. Magnetic resonance image (MRI): considerations and applications in radiotherapy treatment planning. *Radiother Oncol* 1997, 42: 1-5.

FIGURE LEGENDS

Figure 1. A case in which the AVM target was delineated on coregistered contrast-enhanced CT, contrast-enhanced MRA, and CTA (**arrow**). Target on AP and LR view of stereotactic angiography are also shown (**arrow head**).

Figure 2. Distributions of the displacement of centers between MRA-based AVM and angiography-based AVM in LR direction (**a**), in AP direction (**b**), and in CC direction (**c**).

Figure 3. Three-dimensional displacement of MRA-based AVMs from angiography-based AVMs in relation to the maximum diameter of the AVMs

Figure 4. An example of the improvement of the target shape with the information obtained by CTA; (**a**) posterior part of the AVM (**arrow**) was omitted from the target after the integration of the CTA information. (**b**) The resultant beams-eye-view showed good correlation with the LR-view of stereotactic angiography.

Table 1. Characteristics of the material and the results regarding depiction, displacement of center, coverage of angiography-based AVM by MRA-based AVM, and the ellipsoidal volume

	Used images	Location of AVM*	Maximum diameter on angiography (mm)	Depiction of AVM		Displacement of centers of two modalities (mm)				Coverage of Angiography-based AVM by MRA-based AVM (%)			Ellipsoidal volume (cc)	
				MRA†	CTA‡	left-right	anterior-posterior	cranio-caudal	three-dimensional	left-right	anterior-posterior	cranio-caudal	MRA	angiography
AVM-1	MRA only	basal ganglia	48.6	clear	NA	1.1	-0.8	0.8	1.5	100	100	97	49.4	37.8
AVM-2	MRA only	temporal lobe	33.8	clear	NA	-0.7	0.2	-0.7	1.0	100	100	92	8.7	5.3
AVM-3	MRA only	temporal lobe	26.8	clear	NA	-4.0	2.8	1.9	5.2	80	100	100	6.4	3.2
AVM-4	MRA only	pons	36.4	clear	NA	-5.7	-1.4	2.3	6.3	83	96	94	15.7	14.3
AVM-5	MRA only	thalamus	14.7	clear	NA	-1.2	1.2	-0.1	1.7	86	92	100	1.0	0.9
AVM-6	MRA only	temporal lobe	28.9	clear	NA	-1.6	-1.5	3.6	4.2	100	88	92	11.4	10.6
AVM-7	MRA only	cerebellum	20.1	clear	NA	-1.8	-0.5	2.6	3.2	100	100	100	6.9	4.1
AVM-8	MRA only	temporal lobe	13.8	unclear	NA	-2.4	3.8	-0.7	4.5	69	61	94	0.6	1.0
AVM-9	MRA + CTA	temporal lobe	38.2	clear	clear	-2.9	-2.0	-0.1	3.5	86	91	96	10.0	11.8
AVM-10	MRA + CTA	frontal lobe	16.6	clear	clear	-1.4	-1.3	-0.4	2.0	82	97	92	1.3	1.5
AVM-11	MRA + CTA	frontal lobe	19.1	clear	clear	-2.1	-5.1	-0.6	5.6	92	70	84	2.5	2.7
AVM-12	MRA + CTA	temporal lobe	29.8	clear	clear	-12.4	1.6	-1.4	12.5	33	100	96	7.4	7.2
AVM-13	MRA + CTA	occipital lobe	10.3	clear	clear	-1.8	0.5	-0.1	1.9	91	91	100	0.5	0.4
AVM-14	MRA + CTA	occipital lobe	27.3	clear	clear	-0.8	5.6	2.3	6.1	100	70	90	7.5	5.7
AVM-15	MRA + CTA	temporal lobe	27.0	unclear	clear	1.9	-2.4	0.1	3.1	78	100	74	3.4	4.8
AVM-16	MRA + CTA	temporal lobe	27.0	clear	clear	-3.5	0.6	-1.6	3.9	85	93	90	4.6	5.3
AVM-17	MRA + CTA	pons	9.4	clear	unclear	1.5	-1.0	0.6	1.9	100	83	64	0.5	0.3
AVM-18	MRA + CTA	frontal lobe	9.4	unclear	clear	0.4	-0.5	1.4	1.5	100	100	83	0.4	0.3
AVM-19	MRA + CTA	frontal lobe	10.0	unclear	clear	-0.2	0.0	0.0	0.2	98	99	69	0.2	0.3
AVM-20	MRA + CTA	temporal lobe	6.6	unclear	clear	-1.5	-2.8	-0.1	3.2	100	62	100	0.2	0.1
AVM-21	MRA + CTA	pons	12.1	clear	clear	-1.5	3.1	2.7	4.4	81	80	100	1.2	0.6
AVM-22	MRA + CTA	occipital lobe	35.4	unclear	clear	-2.0	-1.0	0.0	2.2	100	100	100	18.7	10.3
AVM-23	MRA + CTA	parietal lobe	44.7	clear	unclear	0.5	7.4	8.6	11.3	88	80	76	27.6	35.7
AVM-24	MRA only	temporal lobe	45.3	clear	NA	-2.0	0.8	4.0	4.5	82	100	88	27.9	30.6
AVM-25	MRA only	cerebellum	67.1	clear	NA	0.0	3.6	-0.1	3.6	92	97	93	97.2	118.1
AVM-26	MRA only	temporal lobe	31.8	clear	NA	-3.7	-3.3	0.4	5.0	99	94	100	15.6	8.9
AVM-27	MRA only	frontal lobe	30.7	unclear	NA	-2.1	-9.0	-2.0	9.4	86	100	83	14.4	11.7
AVM-28	MRA only	temporal lobe	10.7	clear	NA	-1.1	-0.8	2.2	2.6	100	100	100	3.3	0.5

* arteriovenous malformation, † magnetic resonance angiography, ‡ computed tomographic angiography

Table 2. The impact of CTA in addition to MRA for the targeting, regarding the degree of the displacement of centers between MRA(+/- CTA)-based AVMs and angiography-based AVMs

The use of CTA ‡		Distance of centers between angiography-based AVM and MRA(+/-)CT- based AVM (mm)							
		N	LR direction	<i>p</i>	AP direction	<i>p</i>	CC direction	<i>p</i>	3D
no	13	2.07	<i>0.81</i>	3.59	<i>0.37</i>	1.66	<i>0.64</i>	5.32	<i>0.47</i>
yes	15	2.29		2.33		1.33		4.22	

‡ computed tomographic angiography

Figure 1

Aoyama H

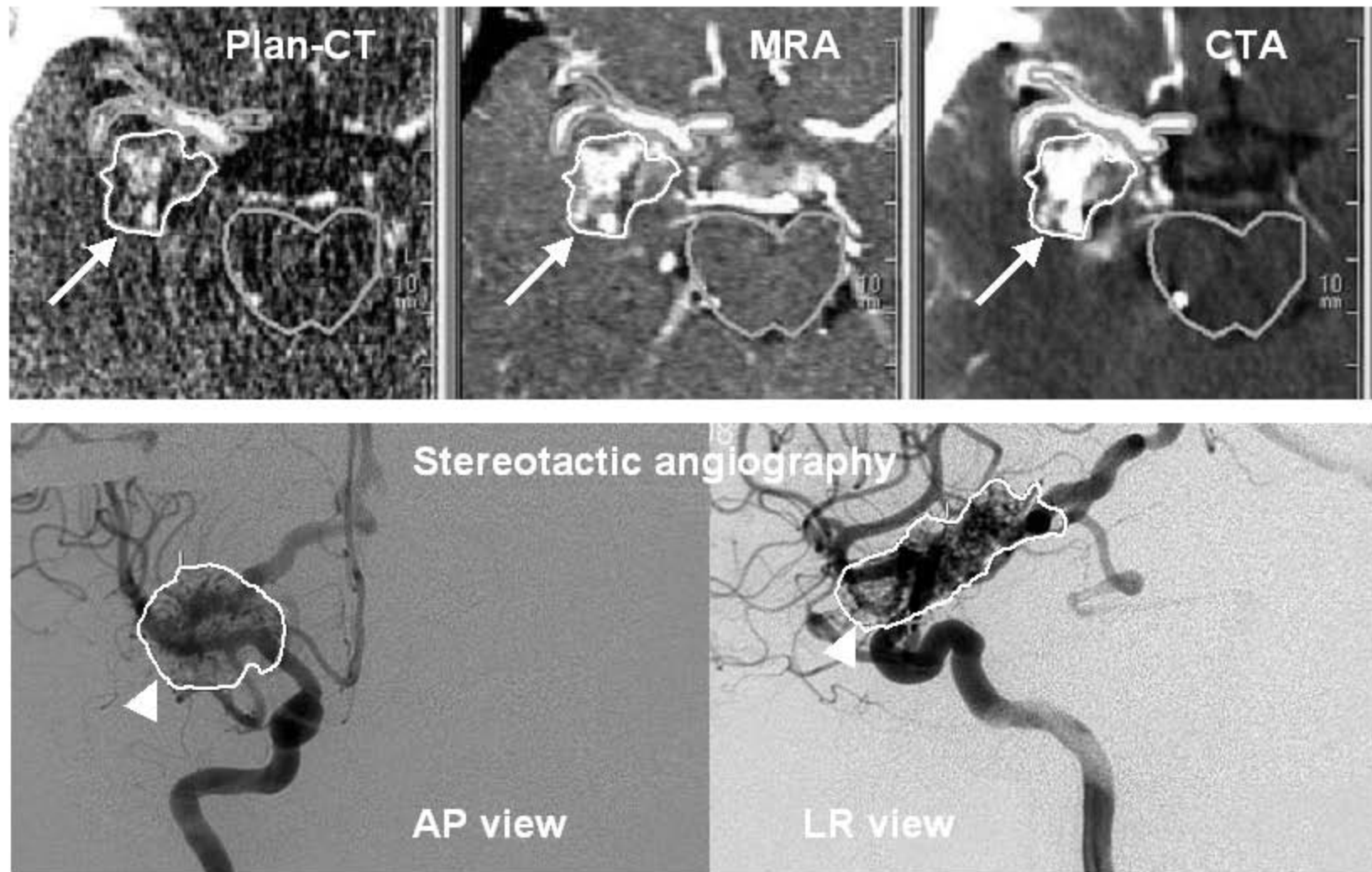


Figure 2a

Aoyama H

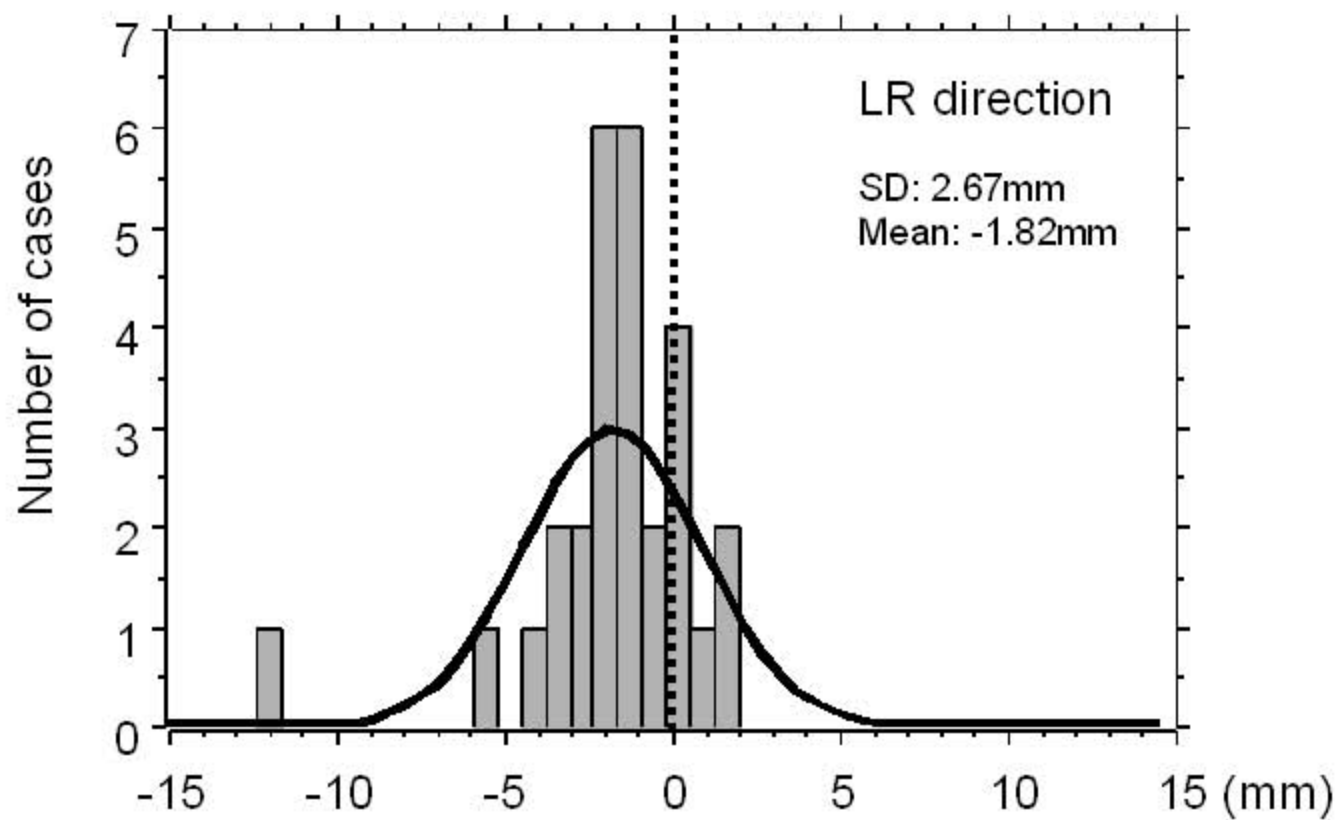


Figure 2b

Aoyama H

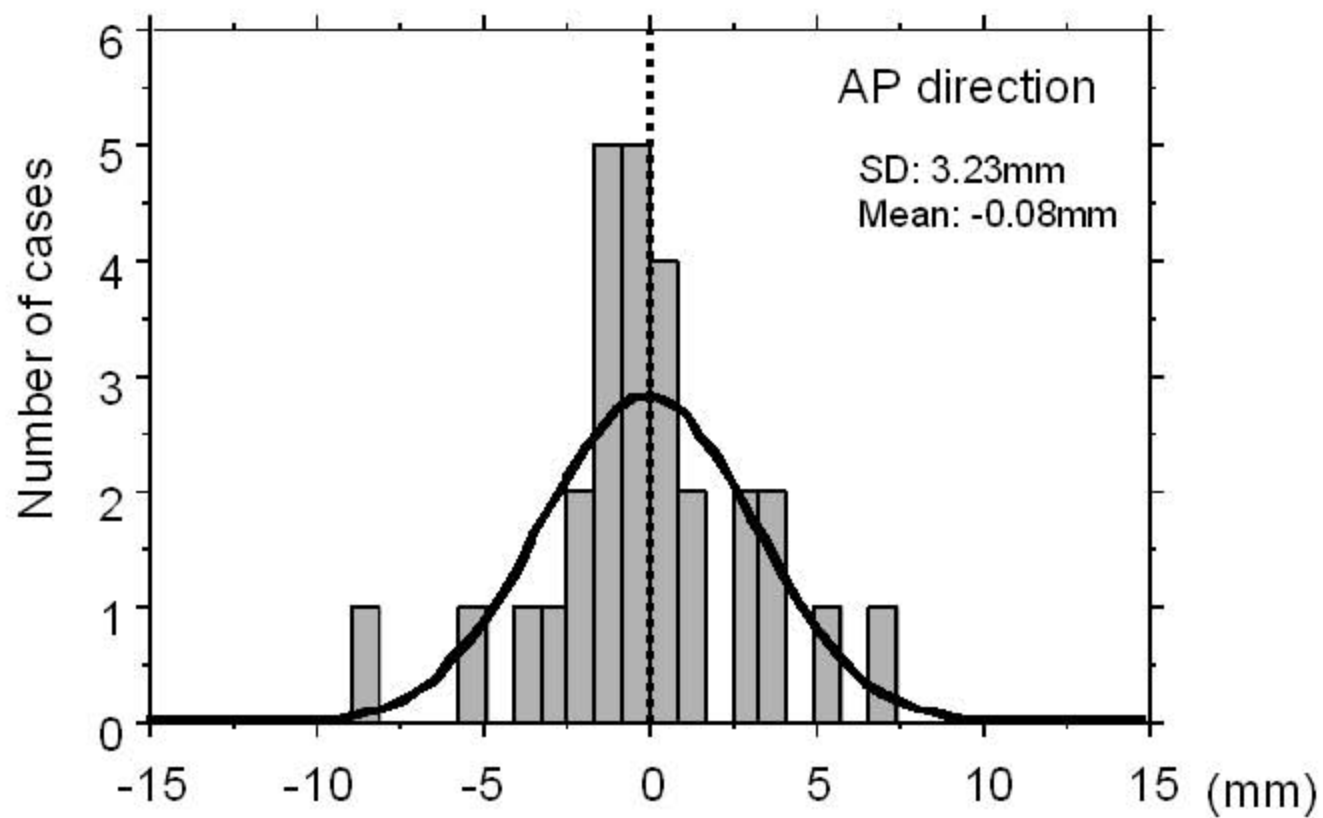


Figure 2c

Aoyama H

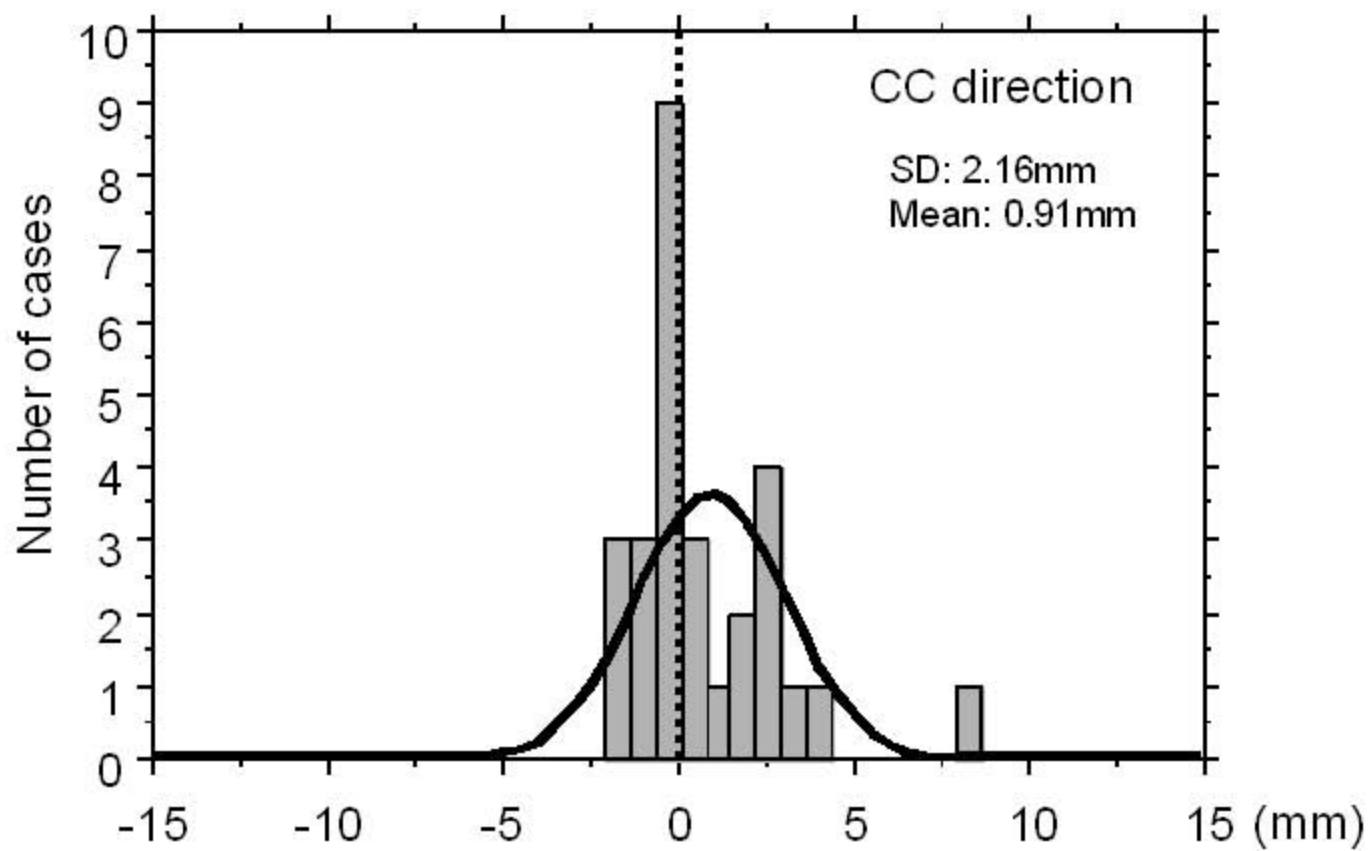


Figure 3

Aoyama H

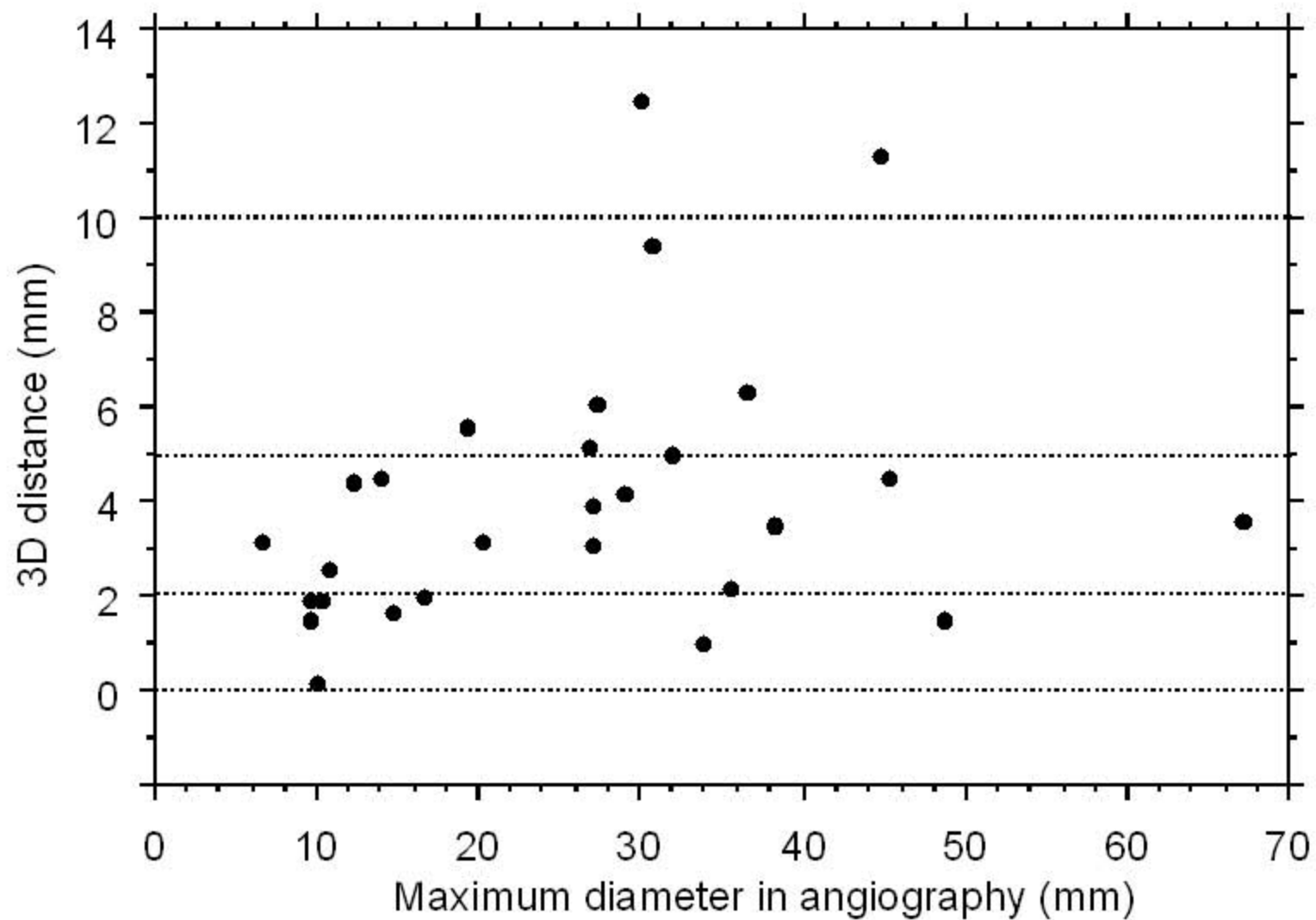


Figure 4a

Aoyama H

